

---

# Learning Debiased Representation via Disentangled Feature Augmentation

---

Eungyeup Kim<sup>\*12</sup> Jungsoo Lee<sup>\*1</sup> Juyoung Lee<sup>2</sup> Jihyeon Lee<sup>1</sup> Jaegul Choo<sup>1</sup>

<sup>1</sup>KAIST, <sup>2</sup>Kakao Enterprise, South Korea

<sup>1</sup>{eykim94, bebeto, gina3833, jchoo}@kaist.ac.kr,

<sup>2</sup>{josh.ey, michael.jy}@kakaenterprise.com

## Abstract

Image classification models tend to make decisions based on peripheral attributes of data items that have strong correlation with a target variable (*i.e.*, *dataset bias*). These *biased* models suffer from the poor generalization capability when evaluated on unbiased datasets. Existing approaches for debiasing often identify and emphasize those samples with no such correlation (*i.e.*, *bias-conflicting*) without defining the bias type in advance. However, such bias-conflicting samples are significantly scarce in biased datasets, limiting the debiasing capability of these approaches. This paper first presents an empirical analysis revealing that training with “diverse” bias-conflicting samples beyond a given training set is crucial for debiasing as well as the generalization capability. Based on this observation, we propose a novel feature-level data augmentation technique in order to synthesize diverse bias-conflicting samples. To this end, our method learns the disentangled representation of (1) the *intrinsic attributes* (*i.e.*, those inherently defining a certain class) and (2) *bias attributes* (*i.e.*, peripheral attributes causing the bias), from a large number of *bias-aligned* samples, the bias attributes of which have strong correlation with the target variable. Using the disentangled representation, we synthesize bias-conflicting samples that contain the diverse intrinsic attributes of bias-aligned samples by swapping their latent features. By utilizing these diversified bias-conflicting features during the training, our approach achieves superior classification accuracy and debiasing results against the existing baselines on both synthetic as well as real-world datasets.

## 1 Introduction

Despite the recent advancement of deep neural networks, they often rely overly on the correlation between peripheral attributes and labels, referred to as *dataset bias* [1], especially when such strong bias is found in a given dataset. A majority of samples in the biased dataset exhibit visual attributes that are not innate but frequently co-occur with target labels (*i.e.*, *bias attributes*). For example, most of the bird images in the training dataset may contain the background as the blue sky, while the birds may still be found in different places. Thus, the model trained with such a biased dataset is likely to learn the bias attributes more than *intrinsic attributes*, the innate visual attributes that inherently define a certain class, *e.g.*, the wings of birds. This causes the model to learn shortcuts for classification [2], failing to generalize on the images with no such correlations (*e.g.*, birds on grounds or grass) during the test phase. Throughout the paper, *bias-aligned* samples correspond to data items containing a strong correlation between bias attributes and labels (*e.g.*, birds on the sky), while *bias-conflicting* samples indicate the other cases that are rarely found (*e.g.*, birds on grounds).

---

\* indicates equal contribution

To tackle such a task, previous studies often define a specific bias type (*e.g.*, color and texture) in advance [3, 4, 5, 6, 7, 8, 9, 10], which enables them to design a debiasing network tailored for the bias. For example, Bahng *et al.* [6] leverage BagNet [11], which has limited size of receptive fields, to focus on learning color and texture. However, defining a bias type in advance 1) limits the capability of debiasing in other bias types and 2) requires expensive labor to manually identify the bias type. To handle such an issue, a recent approach [12] defines a bias based on an intuitive observation that the bias attributes are often *easier* to learn than the intrinsic attributes for neural networks. In this regard, they re-weight bias-conflicting samples while de-emphasizing the bias-aligned ones. However, we point out that the reason behind the limited generalization capability of existing debiasing approaches lies in the significant scarcity of bias-conflicting samples compared to the bias-aligned ones in a given training set. In other words, it is challenging to learn the debiased representation from these scarce conflicting samples because the models are prone to memorize (thus being overfitted to) these samples, failing to learn the intrinsic attributes. Therefore, we claim that a neural network can learn properly debiased representation when these data items are diversified during training.

We conduct a brief experiment to demonstrate the importance of *diversity* in debiasing. Diversity in our work indicates different valid realization of intrinsic attributes in a certain class (*e.g.*, different thickness or tilted degrees of digits in MNIST [13]). Our observation is that training a model with diverse bias-conflicting samples beyond a given training set is crucial for learning debiased representation (Section 3.2). In this regard, synthesizing bias-conflicting samples is one of the straightforward approaches to increase the diversity of such samples. In fact, a large amount of bias-aligned samples in a given training set already contain diverse intrinsic attributes, which can work as informative sources for increasing the diversity. However, as bias and intrinsic attributes are highly entangled in their embedding space, it is difficult to extract the intrinsic ones from these bias-aligned samples. Therefore, disentangling these correlations enables to synthesize diversified bias-conflicting samples that originate from bias-aligned samples.

In this paper, we propose a novel feature augmentation approach via disentangled representation for debiasing. We first train two different encoders to embed images into the disentangled representation of their intrinsic and bias attributes. With the disentangled representation, we randomly swap the latent vectors extracted from different images, most of which are bias-aligned samples in our training set. These swapped features thus contain both bias and intrinsic attributes without the correlation between them, which, in turn, can work as augmented bias-conflicting samples in our training. These features include intrinsic features of bias-aligned ones, increasing the diversity of a given training set, especially for bias-conflicting data items. Furthermore, to enhance the quality of diversified features, we propose a scheduling strategy of feature augmentation which enables to utilize the representation disentangled to a certain degree. In summary, the main contributions of our work include:

- Through our preliminary experiment, we reveal that increasing the diversity of bias-conflicting samples is crucial for debiasing.
- Based on such an observation, we propose a novel feature augmentation method via disentangled representation for diversifying the bias-conflicting samples.
- We achieve the state-of-the-art performances in two synthetic datasets (*i.e.*, Colored MNIST and Corrupted CIFAR-10) and two real-world datasets (*i.e.*, Biased FFHQ and BAR) against existing baselines.

## 2 Related Work

**Debiasing predefined bias** Several existing approaches mitigate the bias by pre-defining a certain bias type, either explicitly [3, 4, 5] or implicitly [6, 7, 8, 9, 10, 14]. For example, Bahng *et al.* [6] and Wang *et al.* [7] design a color- and texture-oriented network to adversarially learn a debiased model against the biased one. However, as these methods still require a specific bias type such as texture, they lack the general applicability to the datasets where the bias types are demanding to recognize.

Instead of defining certain types of bias, recent approaches [12, 15, 16] rely on the straightforward assumption that networks are prone to exploit the bias when it acts as a shortcut [2], *i.e.*, easy to learn in the early training phase. Nam *et al.* [12] emphasize the bias-conflicting samples during training by using generalized cross-entropy loss [17]. Darlow *et al.* [15] and Huang *et al.* [16] presume that high gradient of latent vectors accounts for the shortcuts that model learns. In the line with the recent studies, we tackle debiasing without pre-defining a certain bias type.

Dataset	Diversity ratio	Sampling ratio	Accuracy (%)
Colored MNIST	5%	50%	<b>83.77</b> $\pm$ 2.03
	1%	50%	67.19 $\pm$ 1.99
	5%	1%	<u>77.97</u> $\pm$ 6.00
Corrupted CIFAR-10	5%	50%	<b>46.99</b> $\pm$ 0.82
	1%	50%	33.08 $\pm$ 0.80
	5%	1%	<u>36.66</u> $\pm$ 0.55

Table 1: The classification accuracy on the unbiased test sets. The diversity ratio indicates the ratio of bias-conflicting samples in the dataset pooled for each experiment. Sampling ratio refers to the ratio of bias-conflicting samples included in each mini-batch. We report the averaged accuracy over three independent trials with the standard deviation. In both datasets, we observe that the bias can be mitigated with diverse bias-conflicting samples even with a small sampling ratio. Bold and underlined values indicate the best and second best accuracy, respectively.

**Data augmentation for debiasing** Geirhos *et al.* [10] mitigate the texture bias by utilizing additional training images with their styles being transferred by adaptive instance normalization (AdaIN) [18]. Minderer *et al.* [19] train an image-to-image translation network for removing shortcut cues in the self-supervised task. However, such image-level data augmentation is limited to resolving the predefined texture bias which can not be adopted to other general types of bias.

One alternative is to exploit the latent space for data augmentation. For example, Darlow *et al.* [15] adversarially perturb the latent vectors corresponding to the high gradients to generate the samples against bias. Zhou *et al.* [20] mix the style of different source domains by AdaIN [18] to increase the domain generalization ability. Despite the effectiveness of the augmentation in the latent space, the strong unwanted correlation between bias attributes and labels prevents from obtaining the desirable intrinsic features. We resolve this issue by leveraging the disentangled representation in debiasing, which is widely used in image-to-image translation task [21, 22, 23]. To the best of our knowledge, no previous work in debiasing leverage this disentangled representation for the purpose of feature augmentation. For the rest of the paper, we elaborate how we perform the feature augmentation based on the disentangled representation.

### 3 Importance of Diversity in Debiasing

This section describes the details of a toy-set experiment in which we observe the importance of diversity in learning debiased representation. In Section 3.1, we first introduce the two synthetic datasets, Colored MNIST and Corrupted CIFAR-10, that we utilize for the observation. Then, we elaborate the results of the experiments in Section 3.2.

#### 3.1 Dataset

**Colored MNIST** is a modified MNIST dataset [13] with the color bias. We select ten distinct colors and inject each color on the foreground of each digit to create color bias. By adjusting the number of bias-conflicting data samples in the training set, we obtain four different datasets with the ratio of bias-conflicting samples of 0.5%, 1%, 2%, and 5%.

**Corrupted CIFAR-10** has ten different types of texture bias applied in CIFAR-10 [24] dataset, constructed by following the design protocol of Hendrycks and Dietterich [25]. Each class is highly correlated with a certain texture (*e.g.*, frost and brightness). Corrupted CIFAR-10 also has four different datasets with their correlation ratios as in Colored MNIST.

#### 3.2 Increasing diversity outperforms oversampling

To confirm the significance of diversity of bias-conflicting samples in debiasing, we train three different settings: oversampling bias-conflicting samples by 50% in each mini-batch (*i.e.*, 128 from a batch size of 256), from the pool of i) 5% dataset, ii) 1% dataset and iii) sampling bias-conflicting samples by 1% in each mini-batch (*i.e.*, 2 from a batch size of 256) from the pool of 5% dataset. Oversampling provides the same amount of bias-conflicting samples as the aligned ones to the model

in every training step. Bias-conflicting images sampled from the pool of 5% dataset have more diverse appearances of bias-conflicting samples compared to those from 1% dataset.

Table 1 shows the image classification accuracy of each setting validated on the unbiased test images. Apparently, oversampling diverse bias-conflicting samples (first row) outperforms the other two methods. The interesting finding is that sampling fewer but diverse conflicting samples in each mini-batch (third row) outperforms oversampling bias-conflicting samples with limited diversity (second row). These results lead to the conclusion that the diversity of bias-conflicting samples is a more crucial factor for learning debiased representation than the ratio of sampling in the training. As the diversity is limited (the latter case), the model can be easily overfitted to the given bias-conflicting samples, thus less likely to learn the generalized intrinsic attributes. With Colored MNIST as an example, the model may fail to predict bias-conflicting samples of narrow digits in the test phase when it is trained with bias-conflicting samples mostly composed of thick digits. On the other hand, in the former case, the model can learn multiple visual facets of the bias-conflicting samples (*e.g.*, both thick and narrow digits) when they are sampled from the diverse pool of datasets, resulting in learning intrinsic attributes from them even when they are not oversampled in the training.

## 4 Debiasing via disentangled feature augmentation

Motivated by such an observation in Section 3.2, we propose a feature-level augmentation strategy for synthesizing additional bias-conflicting samples, as illustrated in Fig. 1. First, we train the two separate encoders which embed an image into disentangled latent vectors corresponding to the intrinsic and bias attributes, respectively (Section 4.1). Swapping these feature vectors among training samples enables to augment the bias-conflicting samples which no more contain a correlation between two attributes (Section 4.2). To further enhance the effectiveness, we schedule the feature augmentation after the representation is disentangled at a certain degree (Section 4.3).

### 4.1 Learning disentangled representation

In contrast to the bias-conflicting samples, a large amount of bias-aligned images have diverse appearances of their intrinsic attributes (*e.g.*, tilted digits with diverse degrees in case of the Colored MNIST). By leveraging these attributes for augmentation, we can naturally obtain the diversified bias-conflicting samples containing the diverse intrinsic attributes. However, it remains challenging in that these attributes are strongly correlated with the bias attributes in the bias-aligned samples. Therefore, we propose to design two encoders with their linear classifiers to extract the disentangled latent vectors from the input images.

As shown in Fig. 1, encoders  $E_i$  and  $E_b$  embed an image  $x$  into intrinsic feature vectors  $z_i = E_i(x)$  and bias feature vectors  $z_b = E_b(x)$ , respectively. Afterward, linear classifiers  $C_i$  and  $C_b$  take the concatenated vector  $z = [z_i; z_b]$  as input to predict the target label  $y$ . To train  $E_i$  and  $C_i$  as intrinsic feature extractor and  $E_b$  and  $C_b$  as bias extractor, we utilize the relative difficulty score of each data sample, inspired by the previous work of Nam *et al.* [12]. More specifically, we train  $E_b$  and  $C_b$  to be overfitted to the bias attributes by utilizing the generalized cross entropy (GCE) [17], while  $E_i$  and  $C_i$  are trained with the cross entropy (CE) loss. Then, the samples with high CE loss from  $C_b$  can be regarded as the bias-conflicting samples compared to the samples with low CE loss. In this regard, we obtain the relative difficulty score of each data sample as

$$W(z) = \frac{CE(C_b(z), y)}{CE(C_i(z), y) + CE(C_b(z), y)}. \quad (1)$$

As bias-conflicting samples obtain high values of  $W$ , we emphasize the loss of these samples for training  $E_i$  and  $C_i$ , enforcing them to learn the intrinsic attributes. Therefore, the objective function for disentanglement can be written as

$$L_{\text{dis}} = W(z)CE(C_i(z), y) + \lambda_{\text{dis}}GCE(C_b(z), y). \quad (2)$$

To ensure that  $C_i$  and  $C_b$  predicts target labels mainly based on  $z_i$  and  $z_b$ , respectively, the loss from  $C_i$  is not backpropagated to  $E_b$ , and vice versa.

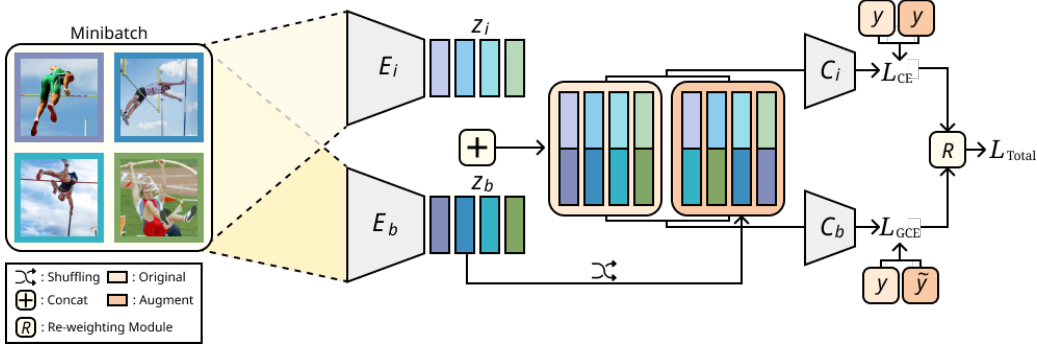


Figure 1: The overview of our proposed debiasing approach.  $(E_i, C_i)$  and  $(E_b, C_b)$  are pairs of an encoder and a linear classifier trained to learn the disentangled representation of intrinsic attributes and bias attributes, respectively. With the disentangled features  $z_i$  and  $z_b$ , the feature augmentation is performed by swapping these latent vectors among different training samples, after certain iterations of training.  $R$  refers to the re-weighting algorithm which implicitly differentiates bias-aligned samples and bias-conflicting samples. Each color indicates the different data samples.

---

**Algorithm 1** Debiasing with disentangled feature augmentation

---

**Input:** image  $x$ , label  $y$ , iteration  $t$ , augment iteration  $t_{\text{swap}}$

Initialize two networks  $(E_i, C_i)$ ,  $(E_b, C_b)$

**while** not converged **do**

    Extract  $z_i, z_b$  from  $E_i(x), E_b(x)$

    Concatenate  $z = [z_i; z_b]$

    Update  $(E_i, C_i), (E_b, C_b)$  with  $L_{\text{dis}} = W(z)CE(C_i(z), y) + GCE(C_b(z), y)$

**if**  $t > t_{\text{swap}}$ :

        Randomly shuffle  $z = [z_i, z_b]$  into  $z_{\text{swap}} = [z_i; \tilde{z}_b]$

        Calculate  $L_{\text{swap}} = W(z)CE(C_i(z_{\text{swap}}), y) + GCE(C_b(z_{\text{swap}}), \tilde{y})$

        Update  $(E_i, C_i), (E_b, C_b)$  with  $L_{\text{total}} = L_{\text{dis}} + \lambda_{\text{swap}}L_{\text{swap}}$

**end**

---

## 4.2 Feature swapping for augmentation

While such an architecture disentangles the intrinsic features and bias features,  $E_i$  and  $C_i$  are still mainly trained with an excessively small amount of bias-conflicting samples. Therefore,  $E_i$  and  $C_i$  fail to fully acquire the intrinsic representation of a target class. To promote further improvement in learning intrinsic feature vectors, we diversify the bias-conflicting samples by swapping the disentangled latent vectors among the training sets. In other words, we randomly shuffle the intrinsic features and bias features in each mini-batch and obtain  $z_{\text{swap}} = [z_i; \tilde{z}_b]$  where  $\tilde{z}_b$  denotes the randomly shuffled bias attributes of  $z_b$ . As the intrinsic and bias attributes in  $z_{\text{swap}}$  are obtained from two different images, they certainly have less correlation compared to  $z = [z_i; z_b]$  where both are from the same image. Since the biased dataset is mostly composed of bias-aligned samples, these vectors are likely from the bias-aligned samples, highly diversified compared to the bias-conflicting ones. Then,  $z_{\text{swap}} = [z_i; \tilde{z}_b]$  act as augmented bias-conflicting latent vectors with diversity inherited from the bias-aligned samples. Along with  $L_{\text{dis}}$ , we add the following loss function to train two neural networks with the augmented features

$$L_{\text{swap}} = W(z)CE(C_i(z_{\text{swap}}), y) + \lambda_{\text{swap}}GCE(C_b(z_{\text{swap}}), \tilde{y}), \quad (3)$$

where  $\tilde{y}$  denotes target labels for shuffled bias attributes  $\tilde{z}$ . Thus, our total loss function is described as

$$L_{\text{total}} = L_{\text{dis}} + \lambda_{\text{swap}}L_{\text{swap}} \quad (4)$$

where  $\lambda_{\text{swap}}$  is adjusted for weighting the importance of the feature augmentation.



Figure 2: Example images of datasets utilized in our work. In each dataset, the first two rows indicate the bias-aligned samples while the third row below the dotted line indicates the bias-conflicting samples. Each column corresponds to the each of the ten classes for Colored MNIST and Corrupted CIFAR-10. Similarly, each two columns and four columns indicate each class for BAR and BFFHQ, respectively.

### 4.3 Scheduling the feature augmentation

While training with additional synthesized features helps to mitigate the unwanted correlation, utilizing them from the beginning of training does not improve the debiasing performance. To be more specific, in the early stage of training, the representations of  $z_i$  and  $z_b$  are imperfectly disentangled to be used as the sources of feature augmentation. Feature augmentation should be conducted after two features are disentangled at a certain degree. Without the disentangled representation, the augmented features work as noisy samples which may aggravate the debiasing performances. We verify the importance of scheduling the feature augmentation in Table 3. Our approach can be summarized with Algorithm 1.

## 5 Experiment

This section demonstrates the effectiveness of feature augmentation based on disentangled representation in debiasing with both quantitative and qualitative evaluation. We compare our method with the previous approaches in debiasing with four different datasets with varied bias ratios. Then, we conduct the ablation study which demonstrates the importance of 1) learning disentangled representation, 2) feature augmentation, and 3) scheduling feature augmentation. For the qualitative evaluation, we verify how our approach disentangles the intrinsic features and bias features by visualizing them on 2D embedding space via t-SNE [26] and reconstructing images from them.

### 5.1 Experiment details

**Baselines** Our baselines consist of vanilla network, HEX [7], ReBias [6] and LfF [12]. Vanilla denotes the classification model trained only with the original cross-entropy (CE) loss, without any debiasing strategies. HEX and ReBias explicitly presume the texture of an image as a bias type, while LfF requires no prior knowledge on it.

**Datasets** As shown in Fig. 2, we use two synthetic datasets (Colored MNIST and Corrupted CIFAR-10) and two real-world datasets (BAR and Biased FFHQ) to evaluate the generalization of debiasing baselines over various domains. Biased action recognition (BAR) [12] is a human action recognition dataset which is biased on places. The classes of BAR are ‘climbing’, ‘diving’, ‘fishing’, ‘racing’, ‘throwing’, and ‘vaulting’. Each action is strongly correlated with its locations (*e.g.*, images of ‘fishing’ are mostly taken at water surfaces). While the original dataset does not include bias-conflicting samples in the training set, we reorganize the validation and test set and include a partial of bias-conflicting samples in the training set for simulating the various degrees of correlation. Biased FFHQ (BFFHQ) is curated from FFHQ dataset [27] which contains human face images annotated with their facial attributes. Among the facial attributes, we select age and gender as the intrinsic and bias attribute, respectively, and construct the dataset with images of high correlation between them. More

Dataset	Ratio (%)	Vanilla [28]	HEX [7]	ReBias [6]	LfF [12]	Ours
		✗	✓	✓	✗	✗
Colored MNIST	0.5	35.19 $\pm$ 3.49	30.33 $\pm$ 0.76	<b>70.47</b> $\pm$ 1.84	52.50 $\pm$ 2.43	<u>65.22</u> $\pm$ 4.41
	1.0	52.09 $\pm$ 2.88	43.73 $\pm$ 5.50	<b>87.4</b> $\pm$ 0.78	61.89 $\pm$ 4.97	<u>81.73</u> $\pm$ 2.34
	2.0	65.86 $\pm$ 3.59	56.85 $\pm$ 2.58	<b>92.91</b> $\pm$ 0.15	71.03 $\pm$ 2.44	<u>84.79</u> $\pm$ 0.95
	5.0	82.17 $\pm$ 0.74	74.62 $\pm$ 3.20	<b>96.96</b> $\pm$ 0.04	80.57 $\pm$ 3.84	<u>89.66</u> $\pm$ 1.09
Corrupted CIFAR-10	0.5	23.08 $\pm$ 1.25	13.87 $\pm$ 0.06	22.27 $\pm$ 0.41	<u>28.57</u> $\pm$ 1.30	<b>29.95</b> $\pm$ 0.71
	1.0	25.82 $\pm$ 0.33	14.81 $\pm$ 0.42	25.72 $\pm$ 0.20	<u>33.07</u> $\pm$ 0.77	<b>36.49</b> $\pm$ 1.79
	2.0	30.06 $\pm$ 0.71	15.20 $\pm$ 0.54	31.66 $\pm$ 0.43	<u>39.91</u> $\pm$ 0.30	<b>41.78</b> $\pm$ 2.29
	5.0	39.42 $\pm$ 0.64	16.04 $\pm$ 0.63	43.43 $\pm$ 0.41	<u>50.27</u> $\pm$ 1.56	<b>51.13</b> $\pm$ 1.28
BAR	1.0	35.32 $\pm$ 0.46	34.18 $\pm$ 0.90	37.02 $\pm$ 0.26	<u>48.15</u> $\pm$ 0.93	<b>52.31</b> $\pm$ 1.00
	5.0	49.91 $\pm$ 0.53	36.26 $\pm$ 0.60	53.25 $\pm$ 0.63	<u>58.81</u> $\pm$ 2.64	<b>63.5</b> $\pm$ 1.47
BFFHQ	0.5	56.87 $\pm$ 2.69	52.83 $\pm$ 0.90	59.46 $\pm$ 0.64	<u>62.2</u> $\pm$ 1.0	<b>63.87</b> $\pm$ 0.31

Table 2: Image classification accuracy evaluated on unbiased test sets of Colored MNIST, Corrupted CIFAR-10, BAR, and BFFHQ datasets with varying ratio of bias-conflicting samples. We denote whether the model requires a bias type in advance by *cross* mark (*i.e.*, not required), and *check* mark (*i.e.*, required). Best performing results are marked in bold, while second-best results are denoted with underlines.

specifically, most of the females are ‘young’ (*i.e.*, age ranging from 10 to 29) and males are ‘old’ (*i.e.*, age ranging from 40 to 59). Therefore, bias-aligned samples which compose the majority of the dataset are young women and old men.

For each dataset, we set the degree of correlation by adjusting the number of bias-conflicting samples among the training dataset. The ratio of bias-conflicting samples are 0.5%, 1%, 2% and 5% for both Colored MNIST and Corrupted CIFAR-10, 1% and 5% for BAR, and 0.5% for BFFHQ, respectively. For the evaluation, we construct an *unbiased* test set which includes images without the high correlation existing in the training set.

**Implementation details** We use multi-layer perceptron (MLP) with three hidden layers for Colored MNIST, and ResNet-18 [28] for the remaining datasets. To accommodate the disentangled vectors, we double the number of hidden units in the last layer of each network. For the training, we set the batch size of 256 for Colored MNIST and Corrupted CIFAR-10, and 64 for BAR and BFFHQ. Bias-conflicting augmentation is scheduled to be applied after 10K iterations for each dataset. We report the averaged accuracy of the unbiased test sets over three independent trials with the mean and the standard deviation. We include the remaining implementation details in Section C.

## 5.2 Quantitative evaluation

**Comparison on unbiased test sets** Table 2 shows the comparisons of image classification accuracy evaluated on the unbiased test sets. In general, our approach demonstrates the superior performance in both synthetic and real-world datasets against the baselines with large gaps. Especially, compared to the baselines which do not define the bias types in advance (vanilla [28] and LfF [12]), our approach achieves the state-of-the-art performance across all datasets. This indicates that utilizing the diversified bias-conflicting samples through our augmentation plays a pivotal role in learning debiased representation regardless of the bias types.

Our approach also outperforms the baselines (HEX [7] and ReBias [6]) which are tailored for a specific bias type (*e.g.*, color and texture) in the real-world datasets. We even show superior performance compared to HEX in Colored MNIST without defining the bias type beforehand. While ReBias achieves the best accuracy in Colored MNIST, they utilize BagNet [11] in order to focus on the color bias. Even without using such an architecture, we achieve the second best performance which is comparable to ReBias.

**Ablation studies** Table 3 demonstrates the importance of each module in our approach through ablation studies: 1) disentangled representation learning, 2) feature augmentation, and 3) scheduling feature augmentation. We set the ratio of bias-conflicting samples to 1% for all experiments. We also compare each module with the vanilla network (first row). We observe that performing the scheduled feature augmentation shows the best classification accuracy on the unbiased test sets across

Disentangle	Augment	Scheduled Augment	Colored MNIST	Corrupted CIFAR10	BAR	BFFHQ
–	–	–	52.09±2.88	25.82±0.33	35.32±0.46	56.87±2.69
✓	–	–	74.03±2.40	27.73±1.02	51.79±1.06	59.4±2.46
✓	✓	–	72.29±3.82	32.81±2.47	49.97±0.66	61.27±3.26
✓	✓	✓	<b>81.73±2.34</b>	<b>36.49±1.79</b>	<b>52.31±1.00</b>	<b>63.87±0.31</b>

Table 3: Ablation studies on 1) disentangled representation learning, 2) feature augmentation, and 3) scheduling feature augmentation. Each row indicates the different training settings with *check* mark denoting the setting applied. We average the accuracy of each training over three independent trials.

all datasets. We also show that performing feature augmentation at the early stage of training does not guarantee the effectiveness of debiasing. For example, in Colored MNIST and BAR, performing feature augmentation at the beginning of training rather aggravates the performance. That is, when the representation of intrinsic attributes and bias attributes are not disentangled at a certain degree, augmented features may act as noisy samples. Training with these additional noisy features prevents models from achieving further improvement.

### 5.3 Analysis

**2D Projection of Disentangled Representation** Fig. 3 shows the projection of latent vectors  $z_i$  and  $z_b$  extracted from the intrinsic encoder  $E_i$  and bias encoder  $E_b$ , respectively, on a 2D space using Colored MNIST. We show projection of  $z_i$  and  $z_b$  in Fig. 3(a) and Fig. 3(b), respectively. The colors of projected dots in the first row (i) and the second row (ii) indicate the target labels and bias labels, respectively. We observe that  $z_i$  are clustered according to the target labels while  $z_b$  are clustered with the bias labels. The results represent that our method successfully learns the disentangled intrinsic and bias attributes.

**Prediction with Disentangled Representation** In Table 4, we report the 1) *original* and 2) *swapping* accuracy of  $C_i$  and  $C_b$ , the linear classifiers of the intrinsic and the bias encoder, respectively. To be specific, for the *original* accuracy, we extract the two disentangled vectors,  $z_i$  and  $z_b$ , from the same image, concatenate them to make  $z = [z_i; z_b]$ , and forward them into each linear classifier. For the *swapping* accuracy, however, we first shuffle  $z_b$  and concatenate  $z_i$  with the shuffled  $z_b$  (*i.e.*, denoted as  $\tilde{z}_b$  in Section 4.2) to make  $z_{\text{swap}} = [z_i; \tilde{z}_b]$ . Then, we pass these concatenated latent vectors to each linear classifier. Afterward, we evaluate the accuracy of predicted labels of 1)  $C_i(z)$  and  $C_i(z_{\text{swap}})$

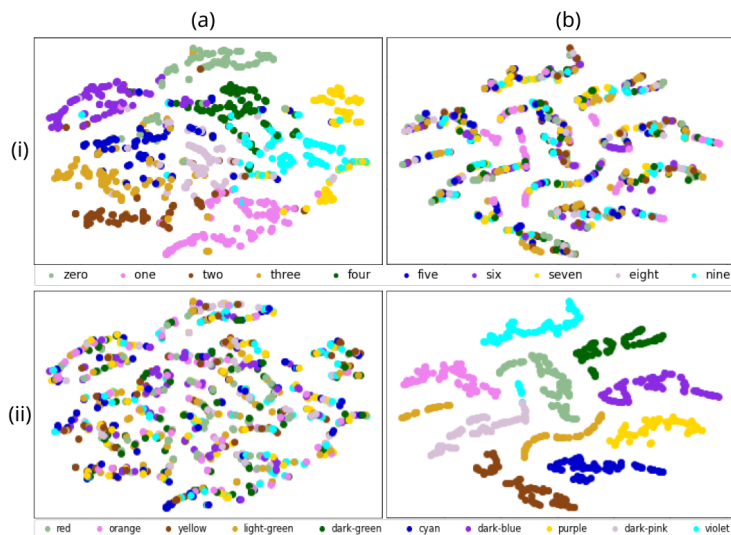


Figure 3: Each row (i and ii) include 2D projection of  $z_i$  and  $z_b$  with the colors encoded by their labels (*i.e.*, groundtruth labels in row i and bias labels in row ii) in Colored MNIST. We observe that  $z_i$  and  $z_b$  are well clustered according to the target and bias labels, respectively.

Accuracy(%)	Colored MNIST		Corrupted CIFAR10		BAR		BFFHQ	
	Intrinsic	Bias	Intrinsic	Bias	Intrinsic	Bias	Intrinsic	Bias
Vanilla	41.63	51.69	24.42	64.29	35.50	–	54.40	45.60
Original	<b>76.08</b>	<b>98.07</b>	<b>35.63</b>	74.16	<b>65.20</b>	–	57.40	49.00
Swapping	71.40	94.29	35.14	<b>76.46</b>	38.96	–	<b>58.40</b>	<b>51.60</b>

Table 4: Accuracy from disentangled representation. The ratio of bias-conflicting samples in Colored MNIST, Corrupted CIFAR-10, BAR, and BFFHQ are 1%, 1%, 5%, and 0.5%, respectively. We did not evaluate with the bias labels of BAR since it does not have explicit bias labels.

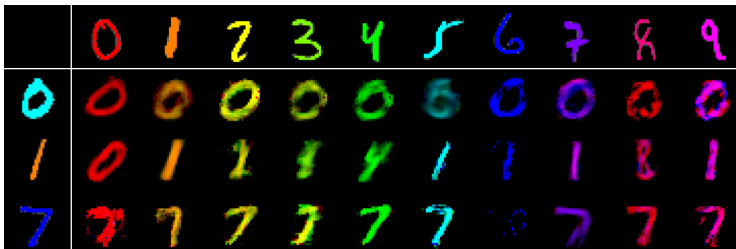


Figure 4: Reconstructed images from disentangled representation in Colored MNIST. Each column and row indicate the samples where the bias attribute (color) and the intrinsic attribute (digit) are extracted, respectively. By swapping the bias features with a given intrinsic feature, we observe that the color changes while maintaining the digit.

with intrinsic labels and 2)  $C_b(z)$  and  $C_b(z_{\text{swap}})$  with bias labels. The *Intrinsic* and *Bias* columns in Table 4 denote the accuracy with respect to the target labels and bias labels, respectively. As the disentangled representations are not available in this vanilla setting, we evaluate it only with the *original* accuracy. We observe that predicting with both disentangled and swapped representation show superior performances compared to vanilla. This indicates that our model well disentangles between  $z_i$  and  $z_b$ , and  $C_i$  robustly utilizes  $z_i$  to predict target labels even when  $z_b$  is taken from the different image, and vice versa.

**Reconstruction of Disentangled Representation** Fig. 4 shows the reconstructed images of Colored MNIST by using the disentangled representation of intrinsic features and bias features. Images in the first row and column indicate the images used for extracting the bias attribute (*i.e.*, color) and intrinsic attribute (*i.e.*, digit), respectively. We train an auxiliary decoder by providing the latent vector  $z$  from our pre-trained models as input in order to visualize the disentangled representations at the pixel level. By changing the bias attributes (as the column changes), the color of digit changes while maintaining the digit shape. This demonstrates that the bias features and intrinsic features independently contain color and digit information, respectively. Note that the reconstruction loss for updating the decoder is not backpropagated to our pre-trained classification models. Due to this fact, the reconstructed images may lack qualities such as showing blurry images. Further implementation details are included in Section C.

## 6 Conclusions

In this work, we propose a feature augmentation method based on the disentangled representation of intrinsic and bias attributes. The main intuition behind our work is that increasing the diversity of bias-conflicting samples beyond a given training set is crucial for debiasing. Since the biased dataset strongly correlates the bias attributes and labels, we intentionally train two different encoders and extract bias features and intrinsic features. After the representations are disentangled to a certain degree, we proliferate the bias-conflicting samples by randomly swapping the vectors. We demonstrate the effectiveness of feature augmentation via extensive experiments, ablation studies, and qualitative evaluation of the disentangled representation. We believe our work inspires the future work of learning debiased representation with the improved generalization capability.

## References

- [1] A. Torralba and A. A. Efros. Unbiased look at dataset bias. *CVPR '11*, 2011.
- [2] Robert Geirhos, Jörn-Henrik Jacobsen, Claudio Michaelis, Richard Zemel, Wieland Brendel, Matthias Bethge, and Felix A Wichmann. Shortcut learning in deep neural networks. *Nature Machine Intelligence*, 2(11):665–673, 2020.
- [3] Byungju Kim, Hyunwoo Kim, Kyungsu Kim, Sungjin Kim, and Junmo Kim. Learning not to learn: Training deep neural networks with biased data. In *The IEEE Conference on Computer Vision and Pattern Recognition (CVPR)*, June 2019.
- [4] Yi Li and Nuno Vasconcelos. Repair: Removing representation bias by dataset resampling. In *Proceedings of the IEEE Conference on Computer Vision and Pattern Recognition*, pages 9572–9581, 2019.
- [5] Shiori Sagawa, Pang Wei Koh, Tatsunori B Hashimoto, and Percy Liang. Distributionally robust neural networks for group shifts: On the importance of regularization for worst-case generalization. *arXiv preprint arXiv:1911.08731*, 2019.
- [6] Hyojin Bahng, Sanghyuk Chun, Sangdoon Yun, Jaegul Choo, and Seong Joon Oh. Learning de-biased representations with biased representations. In *International Conference on Machine Learning (ICML)*, 2020.
- [7] Haohan Wang, Zexue He, Zachary L. Lipton, and Eric P. Xing. Learning robust representations by projecting superficial statistics out. In *International Conference on Learning Representations*, 2019.
- [8] Remi Cadene, Corentin Dancette, Hedi Ben younes, Matthieu Cord, and Devi Parikh. Rubi: Reducing unimodal biases for visual question answering. In H. Wallach, H. Larochelle, A. Beygelzimer, F. d'Alché-Buc, E. Fox, and R. Garnett, editors, *Advances in Neural Information Processing Systems*, volume 32. Curran Associates, Inc., 2019.
- [9] Christopher Clark, Mark Yatskar, and Luke Zettlemoyer. Don't take the easy way out: Ensemble based methods for avoiding known dataset biases. In *Proceedings of the 2019 Conference on Empirical Methods in Natural Language Processing and the 9th International Joint Conference on Natural Language Processing (EMNLP-IJCNLP)*, pages 4069–4082, Hong Kong, China, November 2019. Association for Computational Linguistics.
- [10] Robert Geirhos, Patricia Rubisch, Claudio Michaelis, Matthias Bethge, Felix A. Wichmann, and Wieland Brendel. Imagenet-trained CNNs are biased towards texture; increasing shape bias improves accuracy and robustness. In *International Conference on Learning Representations*, 2019.
- [11] Wieland Brendel and Matthias Bethge. Approximating cnns with bag-of-local-features models works surprisingly well on imagenet. *International Conference on Learning Representations*, 2019.
- [12] Junhyun Nam, Hyuntak Cha, Sungsoo Ahn, Jaeho Lee, and Jinwoo Shin. Learning from failure: Training debiased classifier from biased classifier. In *Advances in Neural Information Processing Systems*, 2020.
- [13] Yann LeCun and Corinna Cortes. MNIST handwritten digit database. 2010.
- [14] Aishwarya Agrawal, Dhruv Batra, and Devi Parikh. Analyzing the behavior of visual question answering models. In *Proceedings of the 2016 Conference on Empirical Methods in Natural Language Processing*, pages 1955–1960, Austin, Texas, November 2016. Association for Computational Linguistics.
- [15] Luke Darlow, Stanisław Jastrzębski, and Amos Storkey. Latent adversarial debiasing: Mitigating collider bias in deep neural networks. *arXiv preprint arXiv:2011.11486*, 2020.
- [16] Zeyi Huang, Haohan Wang, Eric P. Xing, and Dong Huang. Self-challenging improves cross-domain generalization. In *ECCV*, 2020.
- [17] Zhilu Zhang and Mert R Sabuncu. Generalized cross entropy loss for training deep neural networks with noisy labels. *arXiv preprint arXiv:1805.07836*, 2018.
- [18] Xun Huang and Serge Belongie. Arbitrary style transfer in real-time with adaptive instance normalization. In *ICCV*, 2017.
- [19] Matthias Minderer, Olivier Bachem, N. Houlsby, and M. Tschannen. Automatic shortcut removal for self-supervised representation learning. In *ICML*, 2020.
- [20] Kaiyang Zhou, Yongxin Yang, Yu Qiao, and Tao Xiang. Domain generalization with mixstyle. In *ICLR*, 2021.
- [21] Hsin-Ying Lee, Hung-Yu Tseng, Jia-Bin Huang, Maneesh Kumar Singh, and Ming-Hsuan Yang. Diverse image-to-image translation via disentangled representations. In *European Conference on Computer Vision*, 2018.
- [22] Xun Huang, Ming-Yu Liu, Serge Belongie, and Jan Kautz. Multimodal unsupervised image-to-image translation. In *ECCV*, 2018.

- [23] Taesung Park, Jun-Yan Zhu, Oliver Wang, Jingwan Lu, Eli Shechtman, Alexei A. Efros, and Richard Zhang. Swapping autoencoder for deep image manipulation. In *Advances in Neural Information Processing Systems*, 2020.
- [24] A. Krizhevsky and G. Hinton. Learning multiple layers of features from tiny images. *Master’s thesis, Department of Computer Science, University of Toronto*, 2009.
- [25] Dan Hendrycks and Thomas Dietterich. Benchmarking neural network robustness to common corruptions and perturbations. In *International Conference on Learning Representations*, 2019.
- [26] Laurens van der Maaten and Geoffrey Hinton. Visualizing data using t-SNE. *Journal of Machine Learning Research*, 9:2579–2605, 2008.
- [27] Tero Karras, Samuli Laine, and Timo Aila. A style-based generator architecture for generative adversarial networks. In *Proceedings of the IEEE/CVF Conference on Computer Vision and Pattern Recognition (CVPR)*, June 2019.
- [28] Kaiming He, Xiangyu Zhang, Shaoqing Ren, and Jian Sun. Deep residual learning for image recognition. *arXiv preprint arXiv:1512.03385*, 2015.
- [29] Ian Goodfellow, Jean Pouget-Abadie, Mehdi Mirza, Bing Xu, David Warde-Farley, Sherjil Ozair, Aaron Courville, and Yoshua Bengio. Generative adversarial nets. In *Advances in Neural Information Processing Systems*, 2014.
- [30] Alex Krizhevsky. Learning multiple layers of features from tiny images. Technical report, 2009.
- [31] Diederik P Kingma and Jimmy Ba. Adam: A method for stochastic optimization. In *Proc. the International Conference on Learning Representations (ICLR)*, 2015.
- [32] Xudong Mao, Q. Li, Haoran Xie, Raymond Y. K. Lau, Z. Wang, and Stephen Paul Smolley. Least squares generative adversarial networks. *2017 IEEE International Conference on Computer Vision (ICCV)*, pages 2813–2821, 2017.
- [33] Kevin Eykholt, Ivan Evtimov, Earleence Fernandes, Bo Li, Amir Rahmati, Chaowei Xiao, Atul Prakash, Tadayoshi Kohno, and Dawn Song. Robust Physical-World Attacks on Deep Learning Visual Classification. In *Computer Vision and Pattern Recognition (CVPR)*, June 2018.
- [34] Mahmood Sharif, Sruti Bhagavatula, Lujo Bauer, and Michael K. Reiter. Accessorize to a crime: Real and stealthy attacks on state-of-the-art face recognition. In *Proceedings of the 2016 ACM SIGSAC Conference on Computer and Communications Security, CCS ’16*, page 1528–1540, New York, NY, USA, 2016. Association for Computing Machinery.
- [35] Kaylee Burns, Lisa Anne Hendricks, Trevor Darrell, and Anna Rohrbach. Women also snowboard: Overcoming bias in captioning models. *ArXiv*, abs/1803.09797, 2018.
- [36] Pengyu Cheng, Weituo Hao, Siyang Yuan, Shijing Si, and Lawrence Carin. Fairfil: Contrastive neural debiasing method for pretrained text encoders. In *International Conference on Learning Representations*, 2021.
- [37] Paul Pu Liang, Irene Mengze Li, Emily Zheng, Yao Chong Lim, Ruslan Salakhutdinov, and Louis-Philippe Morency. Towards debiasing sentence representations. In *Proceedings of the 58th Annual Meeting of the Association for Computational Linguistics*, pages 5502–5515, Online, July 2020. Association for Computational Linguistics.

This supplementary material presents additional results and descriptions of our approach that are not included in the main paper due to the page limit. Section A shows the reconstructed images of BFFHQ [27] by using the latent vectors of the intrinsic and the bias attributes. Section B presents the qualitative results in terms of the 2D projection of the latent vectors for both the bias and the intrinsic attributes on the biased action recognition (BAR) dataset [12]. Additionally, we conduct an analysis on the clustering of latent vectors along with their original images. Afterwards, we illustrate the implementation details including architecture designs and hyper-parameters for training in Section C. Lastly, Section D briefly discusses broader impacts and limitations of our work in the related field.

## A Reconstruction of Disentangled Representation on BFFHQ

Fig. 5 supplements Fig. 4 by showing the reconstructed images of disentangled latent vectors  $z_i$  and  $z_b$  on BFFHQ. Similar to Fig. 4, columns and rows correspond to those images where the bias attribute (*i.e.*, gender) and the intrinsic attribute (*i.e.*, age) are extracted, respectively. As mentioned in Section 5, we define ‘age’ as either ‘young’ or ‘old’ in our work. The latent vectors extracted from images of each column and row are concatenated to reconstruct their corresponding images, as shown in the middle. While we only utilize a decoder for the Colored MNIST trained with the reconstruction loss in Fig. 4, we also use a discriminator with an adversarial loss [29] to improve the quality of reconstructed images on BFFHQ.

The first row and the column of Fig. 5(a), (b), (c), and (d) indicate the images used to extract the latent vectors of the bias attribute (*i.e.*, gender) and the intrinsic attribute (*i.e.*, age), respectively. Genders of facial images on the leftmost column of Fig. 5(a), (b), (c), and (d) change according to the genders of faces on the top row. For example, in the first column of Fig. 5(a), the male in the second row changes to female in the second column while the female in the third row changes to male in the fifth column. In addition, we observe that the ages of reconstructed images change as the row changes. Note that the highlighted red boxes indicate the representative samples with clear age transitions as the row changes. In the first row of Fig. 5(a), the young female in the second column becomes old in the third row, while the old male in the fifth column becomes young in the second row. These examples verify that both  $z_i$  and  $z_b$  successfully contain the disentangled attributes for ‘age’ and ‘gender’ from each image in the first columns and rows, respectively.

Similar to the decoder used in Colored MNIST, the decoder for BFFHQ is trained independently from our classification models. Due to this fact, the reconstructed samples may seem blurry or include images with less diversity. Table 6 illustrates the architecture we used to reconstruct the images of BFFHQ. We also provide training details of the decoder for BFFHQ in Section C.4.

## B 2D Embedding Visualization of Disentangled Features on BAR Dataset

To supplement Fig. 3, Fig. 6 shows the 2D embedding results of the disentangled latent vectors of bias attributes ( $z_b$ ) and intrinsic attributes ( $z_i$ ), respectively, on the biased action recognition (BAR)

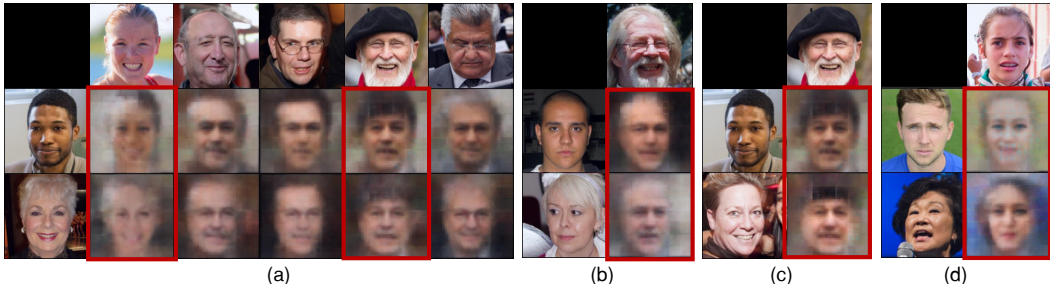


Figure 5: Reconstructed images from disentangled representations on BFFHQ. Columns and rows indicate those samples where the bias attribute (gender) and the intrinsic attribute (age) are extracted, respectively. By swapping the bias features with a given intrinsic feature, we observe that the gender changes while maintaining the age. In addition, by swapping the intrinsic features with a given bias feature, we change the ages while maintaining the gender. The reconstructed images in the highlighted red boxes indicate those samples with obvious age gaps, indicating that the latent vectors are properly disentangled.

dataset [12]. Note that as we do not have groundtruth labels for bias attributes in BAR, we manually select the  $z_b$  clusters with highly distinctive features, as shown in Fig. 6(a) with those corresponding images shown in the enlarged views. Using ground-truth target labels, we select the representative clusters for  $z_i$  in Fig. 6(b).

In Fig. 6(a), images in each cluster share the similar backgrounds. For example, the images of indoor ‘Diving’ with the indoor stadium background are clustered in the top-right corner, while those of outdoor ‘Diving’ with the sky background are clustered in the bottom-left corner. In addition, this cluster on the bottom-left corner includes different types of actions besides ‘Diving’, such as ‘Fishing’ and ‘Throwing’, while sharing similar backgrounds. This indicates that  $z_b$  from our bias encoder  $E_b$  are primarily clustered based on the attributes that are *easy to learn* (i.e., backgrounds) rather than learning the intrinsic attribute (i.e., human action). In contrast, clusters shown in Fig. 6(b) demonstrate that the images of the same action are placed in the same clusters, even with different backgrounds. For example, the top-left cluster includes images of ‘Diving’ taken both indoors and outdoors in the same cluster. Clusters of ‘Vaulting’ (bottom-left), ‘Racing’ (top-right), and ‘Throwing’ (bottom-right) also contain images with a consistent type of human actions, regardless of their backgrounds. From the visualization, we confirm that  $z_i$  contains the innate visual attributes of a particular class while ignoring the bias attributes.

## C Implementation Details

### C.1 Datasets

**Colored MNIST** This biased dataset consists of two highly correlated attributes, *color* and *digit*, following the existing literature [12, 3, 4, 6, 15]. We inject certain color into the foreground of each digit, following Nam *et al.* [12] and Darlow *et al.* [15]. We obtain the total images of bias-aligned samples and bias-conflicting samples for different ratios of bias-conflicting samples: (54,751, 249)-0.5%, (54,509, 491)-1%, (54,014, 986)-2%, and (52,551, 2,449)-5%.

**Corrupted CIFAR-10** We set the corruption types for Corrupted CIFAR-10 dataset in our paper as *Brightness, Contrast, Gaussian Noise, Frost, Elastic Transform, Gaussian Blur, Defocus Blur, Impulse Noise, Saturate, and Pixelate*, among 15 different corruptions introduced in the original dataset [25]. These types of corruptions are highly correlated with the original classes of CIFAR-10 [30], which are *Plane, Car, Bird, Cat, Deer, Dog, Frog, Horse, Ship, and Truck*. Among five different severity of corruptions described in the original paper [25], we use the most severe level of corruptions for our dataset. Following are the total images of bias-aligned samples and bias-conflicting samples for each ratio of bias-conflicting samples: (44,832, 228)-0.5%, (44,527, 442)-1%, (44,145, 887)-2%, and (42,820, 2,242)-5%.

**BAR** This dataset contains the strong correlation between *human action* and the *background* of images, as introduced in [12]. In addition, we sample a small proportion of bias-conflicting samples from the test set and intentionally include them in the training set with different numbers according to the bias ratio, i.e., 1% and 5%. Specifically, for each ratio, we sample 14 and 85 bias-conflicting samples and include them in the training set of 1,761 images.

**BFFHQ** We compose the dataset by utilizing Flickr-Faces-HQ (FFHQ) Dataset [27] along with its various facial information, such as head pose and emotions. Among these features, we choose *age* and *gender* as two attributes with the strong correlation, as mentioned in Section 5. The dataset consists of 19,200 images for training (19,104 for bias-aligned and 96 for bias-conflicting), and 1,000 samples for test.

### C.2 Image Preprocessing

We train and evaluate our model with a fixed size of  $28 \times 28$  and  $32 \times 32$  images for Colored MNIST and Corrupted CIFAR-10, respectively, and  $224 \times 224$  for both BAR and BFFHQ. The images of Corrupted CIFAR-10, BAR, and BFFHQ are preprocessed with random crop and horizontal flip transformations, and also normalized along each channel (3, H, W) with the mean of (0.4914, 0.4822, 0.4465) and standard deviation of (0.2023, 0.1994, 0.2010). For Colored MNIST, we do not use any augmentation techniques to preprocess the images.

Part	Output shape	Layer Information
Input vector	(B, 32)	–
Decoder	(B, 512)	Linear(32, 512), ReLU
	(B, 1024)	Linear(512, 1024), ReLU
	(B, 3 * 28 * 28)	Linear(1024, 3 * 28 * 28), ReLU
	(B, 3 * 28 * 28)	Tanh

Table 5: Decoder architecture used for reconstruction of images from disentangled latent vectors on Colored MNIST. These layers are composed in a reverse order of the MLP encoder used for Colored MNIST. B denotes the batch size.

Part	Output shape	Layer Information
Input vector	(B, 1024, 1, 1)	–
Decoder	(B, 512, 7, 7)	ConvTrans(1024, 512, K7, S2), ReLU
	(B, 256, 14, 14)	ConvTrans(512, 256, K3, S2, P1), ReLU
	(B, 128, 28, 28)	ConvTrans(256, 128, K3, S2, P1), ReLU
	(B, 64, 56, 56)	ConvTrans(128, 64, K3, S2, P1), ReLU
	(B, 64, 112, 112)	Upsampling
	(B, 3, 224, 224)	ConvTrans(64, 3, K3, S2, P1)

Table 6: Decoder architecture used for reconstruction of images from disentangled latent vectors on BFFHQ.

### C.3 Training Details

For training, we utilize Adam [31] optimizer with default parameters (*i.e.*,  $\text{betas} = (0.9, 0.999)$  and  $\text{weight decay} = 0.0$ ) provided in PyTorch library. Learning rates of 0.01, 0.001, 0.001, and 0.0001 are used for training in Colored MNIST, Corrupted CIFAR-10, BAR, and BFFHQ, respectively. For each dataset, we use StepLR for learning rate scheduling, with  $\text{gamma} = 0.1$  and decaying step of 10K. With the proposed scheduled feature augmentation, we start to schedule the learning rate after the feature augmentation was performed. For the proposed objective functions, we use a set of hyper-parameters ( $\lambda_{\text{dis}}, \lambda_{\text{swap}_s}, \lambda_{\text{swap}_c}$ ) as (10.0, 10.0, 1.0) for Colored MNIST, (5.0, 5.0, 1.0) for Corrupted CIFAR-10, (2.0, 2.0, 5.0) for BAR, and (2.0, 2.0, 0.1) for BFFHQ, respectively. We conduct our experiments mainly using a single RTX 3090 gpu.

### C.4 Decoder for image reconstruction

This section provides a detailed explanation of the decoder used for reconstructing images from our disentangled latent vectors, described in Section 5.3 and Section A. The architectures of the decoder for Colored MNIST and BFFHQ are shown in Tables 5 and 6, respectively. For Colored MNIST, we use the mean squared error for the reconstruction loss between the original and generated images, and Adam [31] optimizer with its learning rate of 0.001. For BFFHQ, in addition to the reconstruction loss, we utilize adversarial loss, as proposed in LSGAN [32]. In this respect, we train a discriminator which has the same architecture as our encoder, *i.e.*, ResNet18 [28]. We use Adam optimizer with the learning rate of 0.001 for training the decoder and the same optimizer with 0.0001 for the discriminator, respectively. For every iteration, the decoder takes latent vectors extracted from our encoders as inputs and generates the reconstructed images as outputs. Since we utilize the decoder for the purpose of visualization, the losses of the decoder and the classification models are not backpropagated to each other.

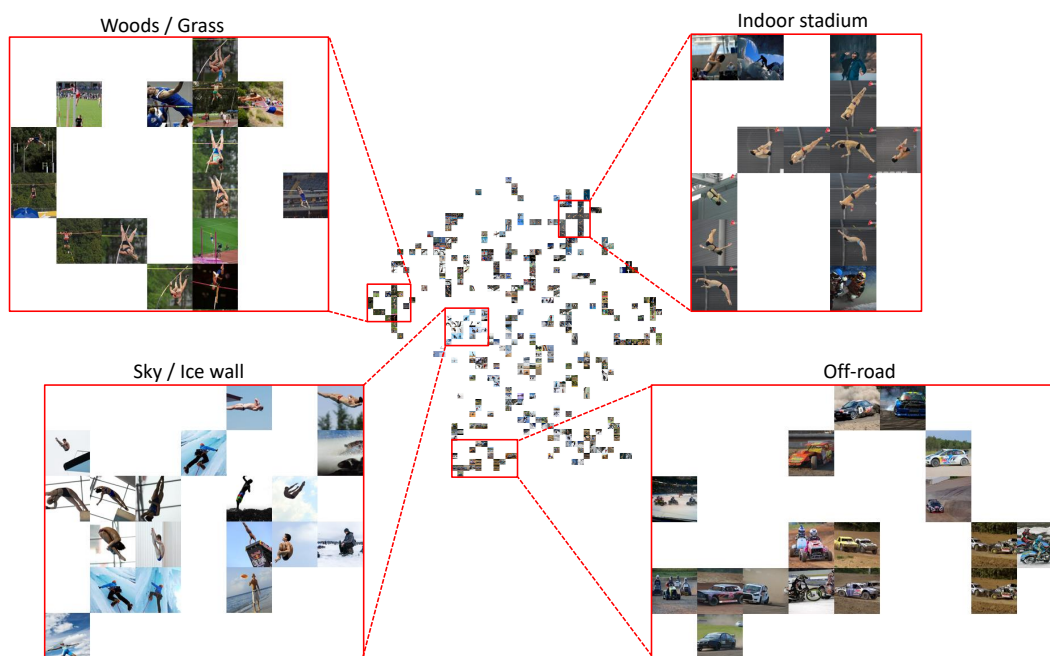
## D Broader Impacts and Limitations

As machine learning becomes a crucial part of our daily life in various forms of applications, it is crucial to validate the robustness and reliability of machine learning models. The dataset bias [1] causes the model to be susceptible to the peripheral features, rather than capturing the intrinsic features that humans usually rely on in image classification. This could raise a distrust issue of machine learning in various tasks sensitive to the safety concern [33, 34] or social equality [35, 36, 37]. Thus, as previous literature has pointed out [12, 3, 4, 6, 5, 19, 7, 16], it becomes important to build

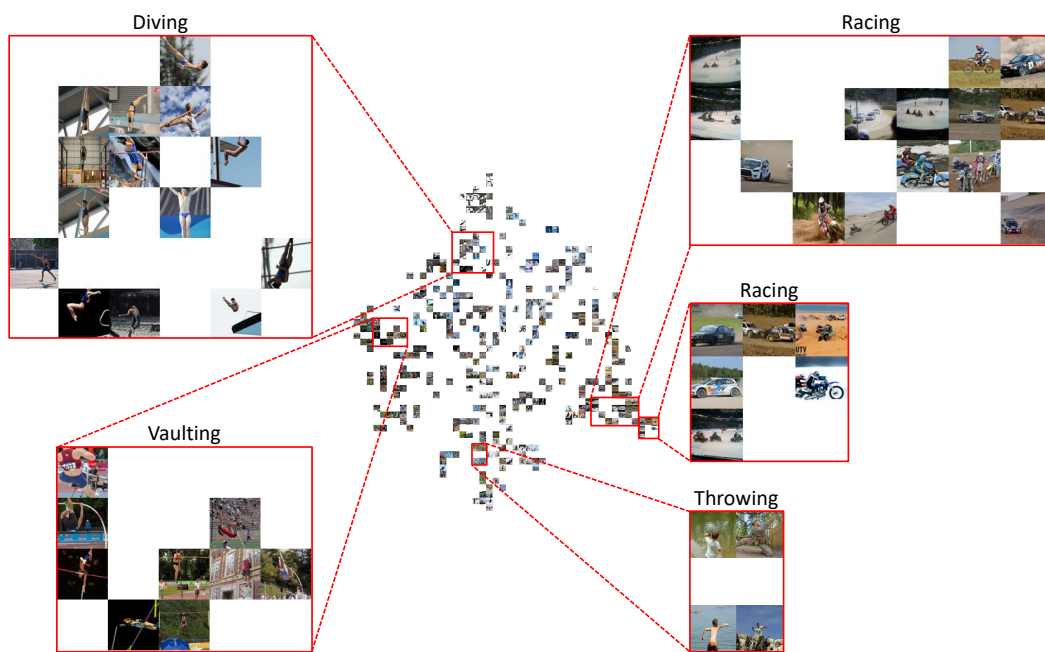
classification models that do not rely on bias attributes but rather learn the intrinsic attributes of a particular class.

Existing approaches address this issue by emphasizing bias-conflicting samples or suppressing the training of bias-aligned images, in order to avoid overfitting to the biased representations. However, as mentioned before, an extremely scarce number of bias-conflicting samples prevent the model from learning the generalizable intrinsic attributes of a certain class. In this paper, we propose an augmentation-based debiasing approach, fully utilizing a large proportion of bias-aligned features to diversify the visual features of bias-conflicting samples. Thus, we achieve the state-of-the-art debiasing performance on both synthetic and real-world datasets against existing baselines.

As a limitation, we acknowledge that learning completely disentangled representations by the proposed method remains challenging, as shown in Table 4. The difficulty derives from the extreme scarcity of bias-conflicting samples and the highly correlated complex attributes in real-world images such as age and gender. Obtaining fully disentangled latent vectors for feature augmentations may further require hand-crafted modules for certain bias types, which is out of scope in this paper since we do not pre-define a bias type in advance. Despite such a limitation, we believe that our approach provides a novel perspective of augmenting diversified bias-conflicting samples for learning debiased representations.



(a)



(b)

Figure 6: 2D embedding of the bias latent vectors  $z_b$  (a) and that of the intrinsic latent vectors  $z_i$  (b). For both cases, we provide the enlarged views of images from the clusters with distinctive visual aspects. Details are better shown by zooming in the figure.